Article

Mechanical Responses of Slurry Shield Underpassing Existing Bridge Piles in Upper-Soft and Lower-Hard Composite Strata

Jianbing Lv [1] , **Dijin Lin** [1] , **Weijun Wu** [1] , **Juan Huang** [1,*] , **Zikun Li** [2] , **Helin Fu** [2] and **Hongzhong Li** [3]

1   School of Civil and Traffic Engineering, Guangdong University of Technology, Guangzhou 510006, China; ljb@gdut.edu.cn (J.L.); 2112109121@mail2.gdut.edu.cn (D.L.); 2112009025@mail2.gdut.edu.cn (W.W.)
2   School of Civil Engineering, Central South University, Changsha 410007, China; lzkcsu1230@126.com (Z.L.); fu.h.l@csu.edu.cn (H.F.)
3   Guangdong Province Communications Planning & Design Institute Co., Ltd., Guangzhou 510507, China; lihongzhong01@126.com
*   Correspondence: cvjuanhuang@gdut.edu.cn; Tel.: +86-139-2628-8216

Abstract: With the development of urban metro systems, shield tunnels that pass through existing bridge pile foundations have become an inevitable engineering problem. Therefore, ensuring the stability of the strata and existing bridge piles during tunnel construction is a common goal in engineering practice. Currently, research on the mechanical responses of strata and existing piles under different conditions of upper-soft and lower-hard composite strata during shield tunneling has not been conducted extensively. This paper presents a numerical simulation of a shield tunnel passing through an existing bridge pile foundation in upper-soft and lower-hard composite strata. Subsequently, the surface subsidence and mechanical responses of a single pile were analyzed and evaluated. Additional stresses generated in the soil by existing bridge piles and the selection of grouting pressure were considered to optimize the driving pressure of the slurry shield. Allowable values were proposed to evaluate the construction disturbances caused by the tunnel excavation. The results show that the disturbance to the soil and existing piles is significantly influenced by the hard-rock height ratio, and the surface subsidence increases when the hard-rock height ratio decreases. The displacement and internal force of a single pile are significantly influenced by the load applied to the pile. This study demonstrates the changes in the mechanical responses of a single pile during shield tunnel boring, and provides in-depth insights into the deformation control caused by shield underpassing structures in upper-soft and lower-hard composite strata.

Keywords: shield tunnel; existing bridge piles; mechanical response; driving pressure; grouting pressure; composite strata

1. Introduction

In the designing and planning of urban metro systems, the penetration of various buildings is inevitably owing to the expansion of underground transportation development. The majority of the buildings in the cities are deep foundation structures. The construction disturbance when the shield penetrates the pile foundation will not only cause surface settlement, but will also lead to the reduction of the bearing capacity of the existing pile foundation, which will affect the working life and the safety of the existing buildings. The impact on the existing pile foundations will be even greater when the shield is bored in composite strata. The impact of subway tunnel construction on the pile foundation is mainly attributed to the driving disturbance that changes the mechanical state of the surrounding strata and the original stress equilibrium, causes the stress to grow, and induces change in the soil. It causes the strata to move and deform. Accordingly, the soil will then transfer the deformation to the neighboring pile foundation. Therefore, the study of the mechanical response of the existing piles subject to the influences of different geological, shield tunneling surface distributions can help actual projects develop

effective construction control measures, and can also allow the control of the deformation of the piles and the surface structure within a safe range when combined with appropriate reinforcement means.

Many scholars have conducted studies on the mechanical responses of shields underpassing pile foundations. These include (among others) theoretical [1–3], experimental [4–7], and numerical simulation studies [8–10]. Zhao [11] analyzed the lateral and axial responses of pile foundations owing to tunnel excavation using a two-stage method. Li [12] investigated the effect of tunnel construction on pile mechanical responses based on a finite element model considering an anisotropic soil model. The computed results indicated that piles with a deeper buried depth and higher stiffness are more capable of mitigating the influence of tunnel excavation. Ma [13] analyzed the displacement of the surrounding soil and adjacent bridge piles subjected to the influence of shield tunneling, and the floating effect of soil together with bridge piles was observed in this study. Mirsepahi Mehrad [14] analyzed the pile foundation response at Z/L_p = 0.8 (near the pile tunnel) and Z/L_p = 1.2 (tunnel below the pile top) to evaluate the effects of different tunnel depths on the pile foundation. Mo [15] proposed a unified clay–sand model based on cavity expansion and shrinkage drainage solutions for tunnel–soil–pile interactions by using cavity expansion analysis to evaluate the effect of pile installation on ground stress, and to determine the pile-end bearing and axial friction distribution. The results of this study indicated that the load capacity degradation and settlement of a pile can be predicted properly when a constant load was applied on a pile. Loganathan [16] studied the effects of tunnel construction on a group of four adjacent piles using a centrifugal trial method, and showed that the lateral displacements and additional bending moments generated by the pile foundations were greater when the tunnel axis was at the same height as the pile ends, which was consistent with the results of study conducted by Ma [13]. Huang [17] studied the influence of tunnel excavation on bridge pile foundations through a finite element model by taking account of groundwater seepage. The results showed that when underpassing piles, the piles above the top of the tunnel settled while the lower piles floated upward. Soomro [18] presented several centrifugal model tests and a corresponding three-dimensional finite element model to study the effects of twin tunnels' excavation on existing piles. A comparison between the computed and measured results indicated that the construction sequence of the twin tunnels had a significant impact on the settlement, inclination, and lateral displacement of the existing piles. Boonsiri [19] investigated the movement pattern of sand surface and subsurface soil layers when two groups of piles of different lengths were set on both sides of the tunnel, based on two-dimensional tunnel model tests. Abuallan [20] proposed a physical model to study tunnel–pile–soil interactions. To simulate the field conditions, pile-hole sand-box experiments were conducted. In this model, the ground surface subsidence and the mechanical responses of a single pile foundation were investigated. The results showed that with a higher excavation speed, both of them were affected more obviously. Soomro [21] conducted a 3D, coupled-consolidation, numerical parameter study to investigate further the effects of a double-sided tunnel excavation on the response of monopiles in saturated hard soils. Ng [22] investigated the effects of the double tunneling sequence on existing piles in dry sand by means of 3D centrifugal model tests and numerical inverse analysis.

According to the literature listed above, it can be observed that the technologies related to the deformation control of subway shield tunnels through pile foundations have become relatively mature, and the mechanism of deformation of the soil and adjacent pile foundations caused by shield construction has been studied in depth. However, most of the scholars selected typical sections of shield tunnels to analyze the mechanical response of the pile foundation. There is no in-depth research on the change of the mechanical properties of the pile foundation caused by dynamic changes of the strata during shield tunnel boring, and there is still relatively little research on the influence control of shield crossing pile foundation in the upper-soft and lower-hard composite strata. Against the preceding background, a numerical study on the surface subsidence and mechanical responses of a single pile during tunnel excavation under different hard-rock height ratios and different

load levels in the composite strata has been conducted in this paper. To evaluate the construction disturbance induced by tunnel excavation, allowable values of displacement have been determined according to requirements for disturbance control. The regularities obtained in this paper are conducive to the disturbance control of shield construction in composite strata.

2. Theory on Impact Control for Shield Underpassing Deep Foundation Buildings Subjected to Complex Geological Conditions

2.1. Definition of Hard-Rock Height Ratio at Shield-Boring Face

Upper-soft and lower-hard composite strata are very common stratigraphic conditions in the construction of shield tunnels with medium burial depths, such as the urban metro. In some areas, the geological distribution of the overburden layer of urban metro tunnels may change with the tunnel line, owing to the wide distribution and undulation of limestone, thus resulting in different proportions of hard rock in excavation faces. To investigate the effects of different hard-rock ratios in shield excavation faces on the deformation of underpassing structures and the strata, the hard-rock height ratio of shield boring faces should be defined.

$$\beta = \frac{D - h}{D} \tag{1}$$

where β is the hard-rock height ratio, h is the height of the soft-rock layer, D is the total height of the tunnel's boring working face, and D is the diameter of the circular tunnel, as shown in Figure 1.
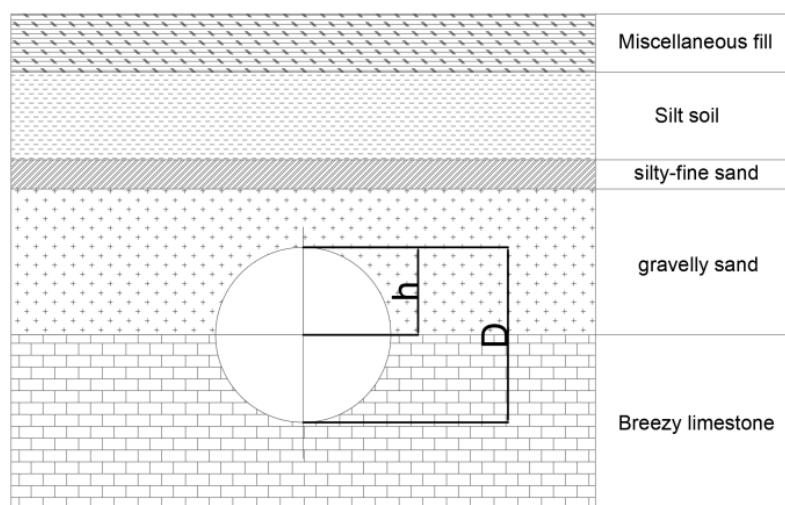

Figure 1. Schematic diagram of hard-rock height ratio.

2.2. Calculation of Additional Stress on Buildings (Structures) in the Shield Underpassing Area

When the shield tunnel crosses the existing bridge piles, the stress state of the shield tunnel will change due to the additional stresses generated by the bridge piles. To ensure the safety of the penetrated body, the boring parameters should be reasonably set to prevent serious construction disturbances. Variations in building morphology, distribution forms, foundation depths, and crossing routes will have an impact on the additional stress of the strata in the underpass area. As mentioned previously, the magnitude of the pile top load is one of the variables considered in this study. Therefore, additional stresses induced by the load applied on piles should be taken into account to properly determine the grouting pressure of the shield tunneling construction. The additional pressure at the base is typically regarded as a local load which acts on the surface of an elastic semi-infinite body, and is calculated in accordance with elastic theory.

As shown in Figure 2, when the uniform strip load P (distributed width b) is applied to the soil surface, the vertical stress σ_z at each point can be calculated using Flamant's equation [23] listed below,

$$\sigma_z = P\alpha_u \tag{2}$$

$$\alpha_u = \frac{1}{\pi}\left[(\arctan\frac{1-2n}{2m} + \arctan\frac{1+2n}{2m}) - \frac{4m(4n^2 - 4m^2 - 1)}{(4n^2 + 4m^2 - 1)^2 + 16m^2}\right] \tag{3}$$

where P is the uniform strip load applied to the soil surface, coefficient α_u is the stress factor which is related to $n = x/b$ and $m = z/b$, and b is the distributed width of the uniform strip load. Parameter n is the ratio of the horizontal distance from a specific point to the coordinate origin to the width of the load distribution. The corresponding value of α_u can be obtained from a table according to parameters n and m. In addition, coordinate values x and z are the horizontal and vertical distances, respectively, from a particular point to the coordinate origin.
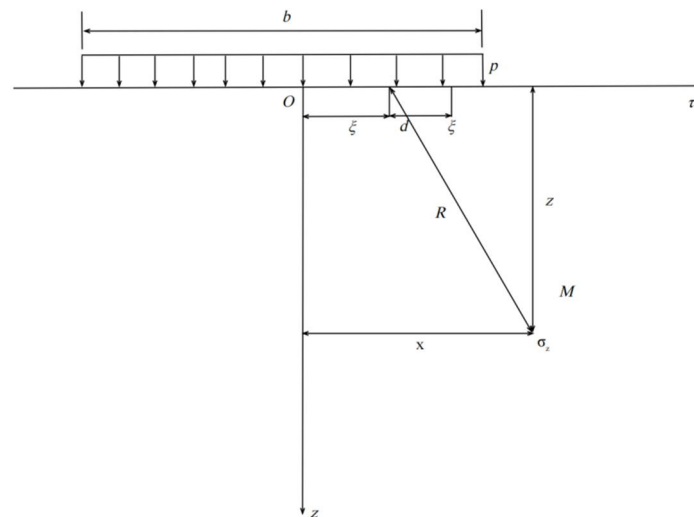

Figure 2. Schematic diagram of stress calculation in soil under uniform strip load.

2.3. Control of Shield Tunneling Construction Parameters

Shield construction is directly influenced by the excavation parameters, which include (among others) driving and grouting pressures, and grouting volume. The influences of different factors vary. Among them, the driving pressure is a very critical one, exerts a considerable impact on the stability of the excavation surface, and subsequently leads to problems related to deformation. In addition, synchronous grouting has influences on the tunnel structure and ground deformation. The subsequent section is an analysis of the influence of these factors, followed by parameter settings so as to control the soil deformation within a reasonable range.

(1)　Driving Pressure

In shield underpassing projects, the driving pressure should be considered together with the pressures of the oil, water, additional stresses, and the net base.

(i)   Soil and Water Pressures

In a slurry shield, the balancing function of the slurry ensures the stability of the boring surface. During construction, the soil pressure in the shield pressure chamber must be maintained at values which exceed the sum of the soil and water pressures of the stratum. For the slurry pressure, the upper limit is set at the static soil pressure, and facilitates the effective control of the ground settlement. The lower limit is the active soil pressure, thus allowing a certain amount of settlement while ensuring the stability of the working surface. The equations for the slurry pressure are listed below.

Upper limit of slurry pressure:

$$P_{\max} = P_0 + P_w + (0.01 \sim 0.02)MPa \tag{4}$$

Lower limit of slurry pressure:

$$P_{\min} = P_a + P_w + (0.01 \sim 0.02)MPa \tag{5}$$

In Equations (4) and (5), P_0, P_a, and P_w represent the static soil, passive soil, and water pressures, respectively (all in megapascals). They are calculated according to the following equations.

(ii)   Additional Stress

The calculations are based on rectangular uniform loads and according to the following equations [23].

$$\sigma_z = \int_0^b \int_0^l \frac{3z^3 P_n dx dy}{2\pi(\sqrt{x^2+y^2+z^2})^5}$$
$$= \frac{P_n}{2\pi} \left[\frac{ij}{\sqrt{1+i^2+j^2}} \left(\frac{1}{i^2+j^2} + \frac{1}{1+j^2} \right) + \arctan\left(\frac{i}{j\sqrt{1+i^2+j^2}} \right) \right] \tag{6}$$
$$= K_s P_n$$

where K_s represents the additional stress factor, which is related to $i = l/b$ and $j = z/b$. The parameters l and b are the length and width of the rectangular uniform load face, respectively. Additionally, P_n stands for the net base pressure, and z is the depth at the center of the working face.

(iii)   Net-base Pressure

The net-base pressure is given by

$$P_n = P - \gamma h, \tag{7}$$

where h represents the burial depth, and P represents the load.

In summary, the calculation of the driving pressure when the shield is underpassing the pile foundation is expressed by the following equation.

$$P_e = P_0 + K_0 K_s P_n, \tag{8}$$

where K_0 stands for the ratio of the horizontal to vertical soil pressure (typically set to 1.0).

(2)   Synchronous Grouting Volume

In actual tunneling, the amount of synchronous grouting will be affected by factors such as grouting pressure, shield curve overcutting, and the soil condition. An accurate calculation of the grouting volume is beneficial to improve the segments' installation quality. The term $(D_1 - D_2)$ in Equation (9) represents the thickness of the grouting layer, which is significant to the simplified simulation of the grouting between the surrounding rock

and the segments. For a single stroke in the shield tunneling, the grouting volume can be calculated by the following equation.

$$Q = \left[\frac{\pi}{4}\left(D_1{}^2 - D_2{}^2\right)\right] La, \tag{9}$$

where L and a represent the stroke length and the grouting rate, respectively. The former is equal to the length of a segment and the latter is usually set to values in the range of 1.3–1.8, according to the relevant standards. Parameters D_1 and D_2 are the cutting diameter of the cutter disc and the outer diameter of the segment (both in meters), respectively.

(3)   Synchronous Grouting Pressure

The static soil and water pressures at the grouting point are typically set at 1.1 to 1.2 times their values. Scholars have conducted studies in this field, and have analyzed the correlation between the surface settlement and synchronous grouting pressure to explore the influence of the latter. It is mentioned in some of the studies that the surface settlement can be reduced effectively when the grouting pressure is basically the same as the formation stress at the buried depth. According to relevant studies, the soil arch effect should be taken into account in the calculation of the soil pressure in certain conditions (H > 2D, h > D) to obtain the results that are more in line with actual situations. Therefore, the calculation can be processed based on Terzaghi's soil pressure theory. In accordance with the theory, the displacement of the soil above the tunnel is affected by the burial depth. In the cases of larger burial depths, it is more likely that deformations will occur in the tunnel's upper area, a depth equal to 1–2 times the upper diameter. The specific calculation is shown in Figure 3. Equations (10) and (11) [23], respectively, show the calculation of the height of the soil arch and the overlying load in which the weight of the shaded part is ignored.
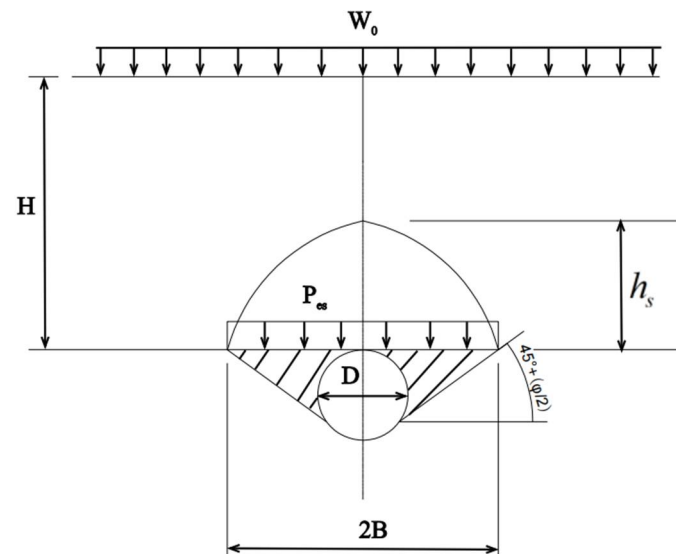

Figure 3. Schematic diagram of overburden earth pressure calculation.

$$P_{es} = \frac{B(\gamma - c/B)}{K_0 \tan \phi}\left(1 - e^{-K_0 \tan \phi \frac{H}{B}}\right) + W_0 e^{-K_0 \tan \phi \frac{H}{B}}, \tag{10}$$

$$B = \frac{D}{2}\cot\left(\frac{45° + \frac{\phi}{2}}{2}\right), \tag{11}$$

In the equations, *H*, *D*, and *B* are the overburden depth, outer diameter of the tunnel, and loosened width above the tunnel (all in meters), respectively. P_{es} is the loose soil pressure in kN/m^2, W$_0$ and c are the ground load and soil cohesion in kPa, respectively, γ is the soil capacitance in kN/m^3, K_0 has the same meaning as in Equation (8), and φ is the internal friction angle in degrees. Additionally, h_s is the height of the soil arching effect.

In addition to the above factors, other factors should be taken into account in setting the synchronous grouting pressure. It must be slightly higher compared with the soil pressure on the outside of the grouting pipe. Additionally, the pressure loss in piping is typically set to 0.2 MPa.

3. Data Simulation of the Shield Underpassing Bridge Piles

3.1. Simulation of Stratigraphy and Structure

This study uses the finite element software Midas GTS NX to simulate the data of the shield tunnel subjected to existing bridge piles. The overall dimensions needed for the establishment of the 3D finite element model were selected to be equal to 90 m in the X-direction, 78 m in the Y-direction, and 25 m in the Z-direction. The following soil layers and structures were considered in the modeling process:

1. Soil layers: The distribution of geotechnical layers of the strata from top to bottom are: miscellaneous fill, silty soil, fine sand, medium to coarse sand, and slightly weathered limestone. The location of the shield palm lied between the medium coarse sand and the slightly weathered limestone, and the groundwater level was set at −4.7 m. Each geotechnical layer was simulated using the Mohr–Coulomb local structure, i.e., its elastic–plastic deformation was considered.
2. Shield segments: The diameter of the shield tunnel tube sheet was 6 m, each section was 3 m long, and a total of 26 sections of tube sheet were simulated for each of the two-lane tunnels, as shown in Figure 4. The shield tube piece should not consider the circumferential stiffness, and cannot ignore the longitudinal stiffness discount situation.

Figure 4. Shield tunnel model.

3.   Grouting layer: To simulate synchronous grouting as accurately as possible, this study used the "equal generation layer" assumption to simulate the grouting layer, i.e., the factors that are difficult to quantify in the grouting process are generalized to obtain a relatively homogeneous "equal generation layer" with the same thickness. At the same time, the hardening process of the cement mortar from low strength (at the beginning of grouting) to high strength (at a later stage), and the decrease of the grouting pressure from the initial value to 0 MPa, were simulated by increasing the strength of the "equivalent layer" and by decreasing the grouting pressure in two steps. In this study, the thickness of the "equivalent layer" for the synchronous grouting of the shield tunnel was taken as $\delta = 0.3$ m.

4.   Bearing platform and pile foundation: The height of the existing bearing platform was 1 m, the length of the infill pile was 7.5 m, the pile diameter was 480 mm, and the group pile arrangement is shown in Figure 5. The distance between the top of the tunnel vault and the bottom of the pile foundation of the bearing platform was 1.4 m.
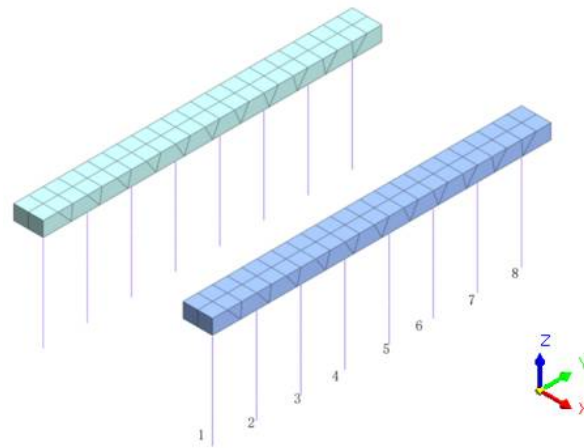

Figure 5. Model of cap and pile foundation.

The parameters of each geotechnical layer and structure are listed in Table 1.

Table 1. Stratigraphic and main material parameters.

Project	Modulus of Elasticity (MPa)	POISSON'S RATIO	Severe (KN/m³)	Cohesive Force (kPa)	Internal Friction Angle (°)
<1> Miscellaneous fill	2.5	0.35	16.5	8	10
<4-2B> Silty sand	5	0.42	17	12.6	12.8
<3-1> Silty-fine sand	12	0.25	20.3	15	35
<3-3> Gravelly sand	40	0.30	19.6	10	30.5
<9C-2> Slightly weathered limestone	10,000	0.30	25	1500	55
Segment	34,500 × 0.7	0.2	25	-	-
Equivalent layer	13	0.3	22.5	-	-
Piles and pile caps	30,000	0.25	25	-	-

3.2. Simulation of Different Hard-Rock Height Ratios at the Shield Tunneling Face

The shield tunneling faces simulated in this section are in medium-coarse sand and slightly weathered limestone, and five shield tunneling faces with hard-rock height ratios β of 0, 0.2, 0.5, 0.8, and 1.0 were selected for simulations in this study, as shown in Figure 6.
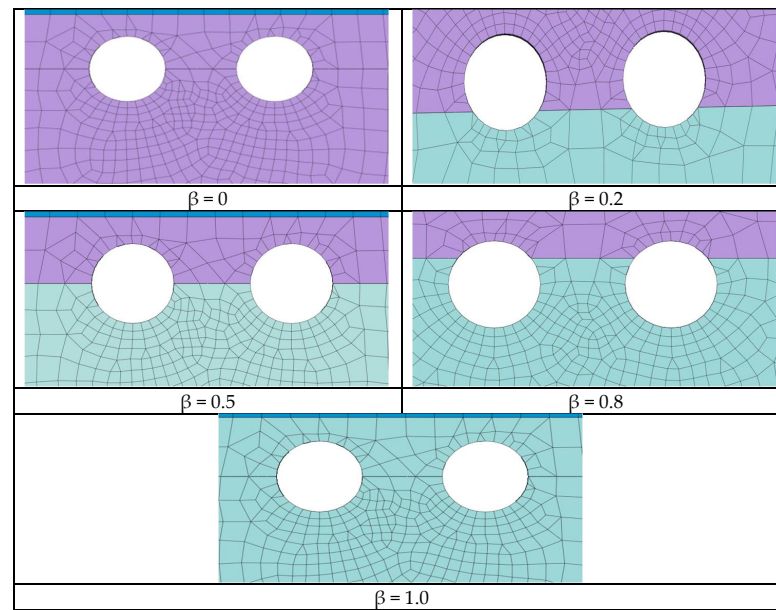
Figure 6. Shield driving face with different ratio of hard-rock height.

3.3. Construction Parameters and Deformation Control

1.　Loads

As shown in Figure 7, this chapter applies distributed loads above the bearing platform with applied load values *p*: 100, 200, and 400 kPa, respectively.

2.　Shield Construction Parameters

During the simulated shield tunneling, the boring and grouting pressures were set according to Equations (8) and (10) for different hard-rock height ratios and pile top loads, as shown in Table 2.

3.　Allowable disturbance

To evaluate the construction disturbance, allowable values of ground settlement, single-pile displacement, and the stress level of a single pile have been proposed according to requirements of engineering practice, as shown in Table 3.
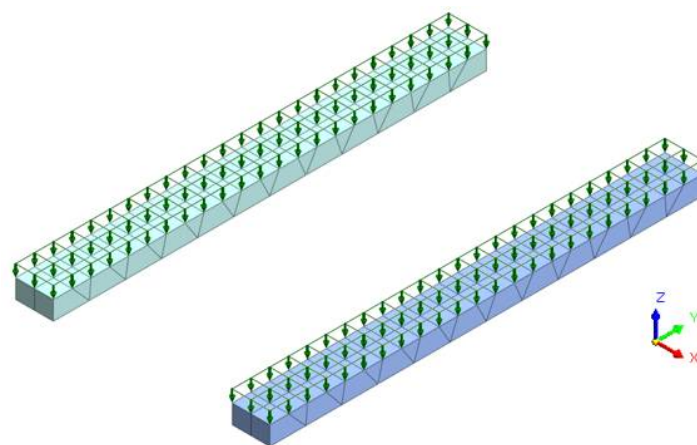
Figure 7. Schematic diagram of superstructure load.

Table 2. Table of shield driving parameters.

β	p (kPa)	Driving Pressure (MPa)	Synchronous Grouting Pressure (MPa)
0	0	0.183	0.122 + 0.2 = 0.322
0.2	0	0.182	0.153 + 0.2 = 0.353
	0	0.180	0.153 + 0.2 = 0.353
	100	0.182	0.193 + 0.2 = 0.393
0.5	200	0.183	0.232 + 0.2 = 0.432
	400	0.186	0.312 + 0.2 = 0.512
0.8	0	0.262	0.153 + 0.2 = 0.353
1.0	0	0.258	0.153 + 0.2 = 0.353

Table 3. Table of allowable values of construction disturbance.

Ground Settlement (mm)	Single-Pile Displacement (mm)	Stress Level of Single Pile (MPa)
−40~+10 mm	2.5 mm in horizontal 10 mm in vertical	1.89 MPa in tensile stress

Note: positive sign in ground settlement represents subsidence; negative sign represents uplift.

3.4. Construction Phase Simulation

The main working conditions simulated in this section included the construction simulation of the existing bearing bridge piles and the excavation simulation of the shield tunnel. The specific construction steps were simulated as follows:

(1) Initial ground stress: All the soil layers were activated at this stage along with the overall model constraints and self-weight. We set the groundwater level to −4.7 m and checked the displacement clearing.

(2) Pile foundation bearing construction simulation: This stage activated the bearing structure, pile foundation, and bearing loads. Given that there was no need to consider the effect of displacement after the completion of the bearing and pile foundation, we checked the displacement clearance.

(3) Simulation of shield tunnel construction: At this stage, two shield tunnel excavations were simulated, namely the right tunnel (first) and the left tunnel (second). Each shield tunnel was 78 m long and was divided into 26 excavation sections.

The model contained 57 construction steps in total, including one bridge construction step, 28 advanced tunneling construction steps, and 28 backward tunneling construction steps. After the above modeling process, the constructed overall finite element model is shown in Figure 8 (hard-rock height ratio of 0.5).
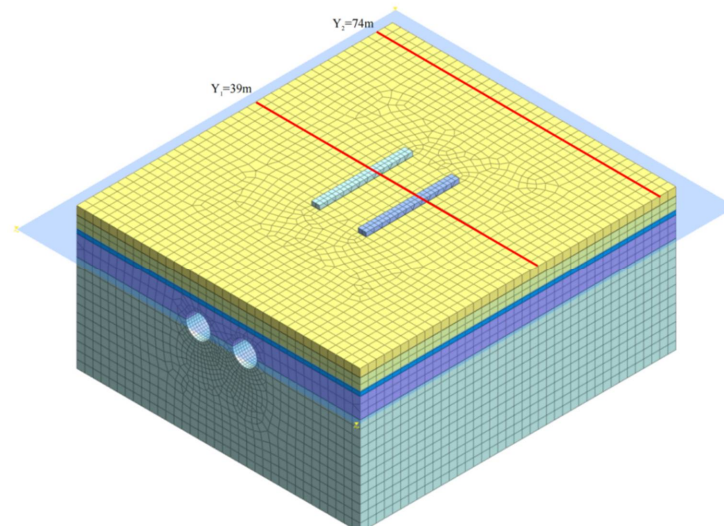
Figure 8. Finite element model.

4. Mechanical Response of Shield Underpassing Bridge Piles at Different Hard-Rock Height Ratios

In this section, an influential analysis of surface settlement, monopile displacement, and internal force variations caused by shield construction was conducted for five different scenarios with hard-rock height ratios β of 0, 0.2, 0.5, 0.8, and 1.0, at the shield excavation face.

(1)   Surface Settlement Analysis

The surface settlement measurement lines are selected as the Y_1 and Y_2 measurement lines in Figure 8, which represent the surface settlement measurement lines inside and outside the area of the underpassing piles, respectively. The final surface settlement values after the completion of the construction of the two-lane shield tunnel are selected for analysis. The final surface settlement curves are shown in Figures 9 and 10. From the curves, it can be observed that as the β value of the shield palm surface decreases, the surface settlement value increases, the depth of the surface settlement trough increases, and the width of the surface area caused by the settlement increased. In the case in which the β value of the palm surface is the same, the settlement value of the underpass area is larger than that outside the area, and the settlement trough is deeper. When the shield palm surface $\beta = 0$, i.e., when the shield is tunneled in the full sand section, the surface outside the underpass area only has one settlement trough, the center of which is at the midpoint between the two tunnels.

When the hard-rock height ratio approaches one, the surface inside the area of the tunnel excavation tends to uplift in the local area, which should be noted in engineering practice. Compared with the allowable values of vertical surface displacement, the surface subsidence is within the allowable range, which is acceptable in practice.
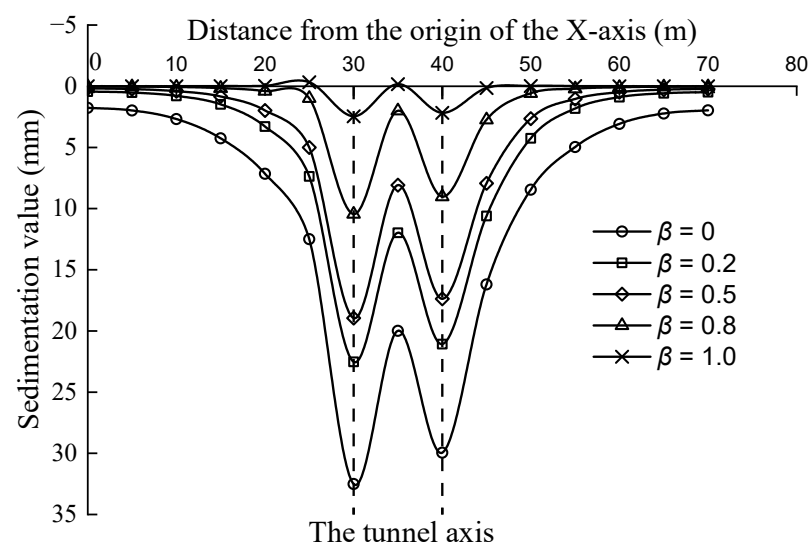

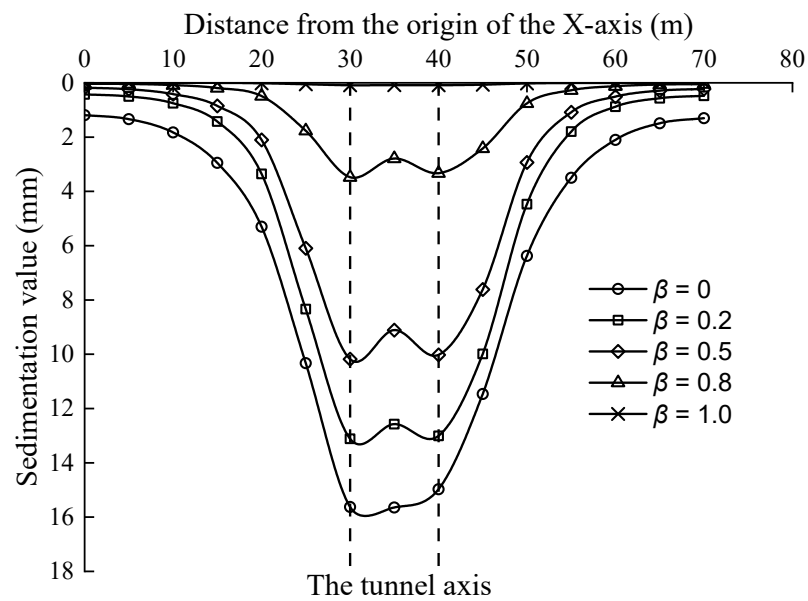**Figure 9.** Surface subsidence curve of line Y1.

Figure 10. Surface subsidence curve of line Y2.

(2)　Single-Pile Settlement Analysis

As shown in Figure 11, the existing piles are above the location of the excavated section 10 to 18 of the right-hand tunnel (S10–S18). A single-pile settlement was selected for analysis from pile No. 5 of the right bearing platform in Figure 6, which is above the excavated section 15 (S15) of the right tunnel. The variation of the pile top settlement of pile No. 5 with the shield underpassing construction is shown in Figure 12.

Figure 12 shows that the bridge pile does not settle when the shield is dug outside the range of 12 m behind the bridge pile, but a small amount of settlement occurred when the shield was dug within the range of 6–12 m behind the bridge pile. When the shield was dug within the range of 6 m behind the bridge pile, the settlement rate of the bridge pile increased when the shield panel approached, and remained after the shield crossed. Furthermore, the settlement value of the bridge piles tended to stabilize after the shield crossed 6 m through the bridge piles. As the β value of the shield palm surface increased, the settlement of the piles caused by the underpassing bridge pile construction decreased. When the β value of the shield palm surface was in the range of 0–0.5, the final settlement value of the bridge piles caused by the underpass construction became closer, and the bridge pile settlement could only be controlled more effectively when β > 0.8. Further analysis and comparison indicate that if no load was applied, safety in construction could be guaranteed only when hard rock accounts for a large proportion. Otherwise, measures of strata reinforcement must be taken before underpass construction.
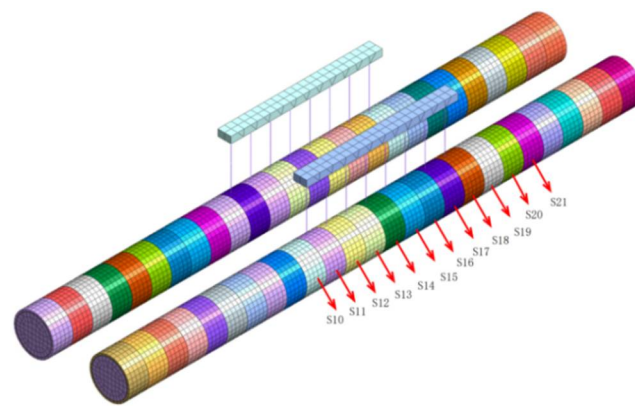
Figure 11. Position diagram of underpass pile for shield tunneling.
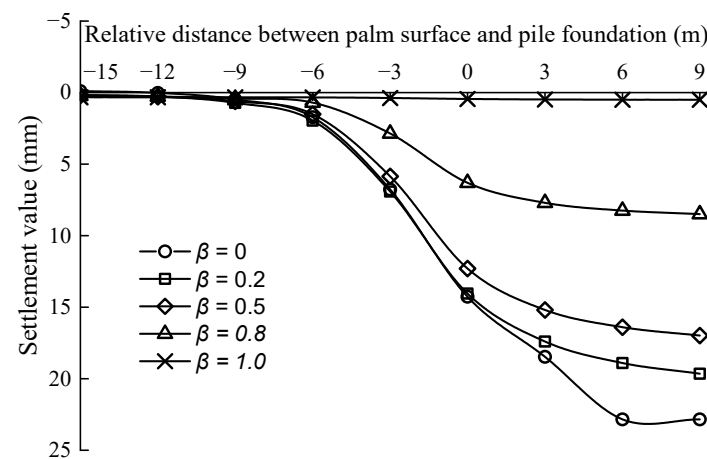

Figure 12. Single pile tip settlement curve.

(3)   Analysis of Horizontal Displacement of Single Pile

Figure 13 shows the horizontal displacement curves of the pile top of pile No. 5 before (S10, S12), during (S14, S15), and after (S16, S18) shield penetration with β = 0.5 at the shield palm surface. It can be observed that the displacement of pile No. 5 in the horizontal direction decreases first and then increases in the reverse direction along the depth direction of the pile. As the underpassing proceeds (S12–S18), the horizontal displacement at the top of the pile decreases first, and then increases in the reverse direction, and the horizontal displacement at the pile end keeps increasing. In the two construction steps at the time of underpassing, the horizontal displacement (within a distance equal to 1/5 of the length above the pile end) increased more as a function of the pile depth. After the shield underpassing, the horizontal displacement at the pile end tended to stabilize.

The final horizontal displacement values of the shield under pile No. 5 in the palm plane with different β values are shown in Figure 14. It can be shown that after the shield is fully excavated and completed, pile No. 5 moves toward the direction of the left line tunnel (negative X-axis direction) at all places, and the displacement decreases as a function of the pile burial depth. The horizontal displacement of the pile will also decrease as a function of the β value, and when β ≥ 0.8, the horizontal displacement of the pile can be negligible.

From Figure 14, it can also be observed that in the case of β = 0.5, the maximum lateral displacement is 2.21 mm, from which it can be predicted that when the hard-rock height ratio is greater than 0.5, the maximum lateral displacement is likely to exceed the allowable value and the risk of construction disturbances may increase.
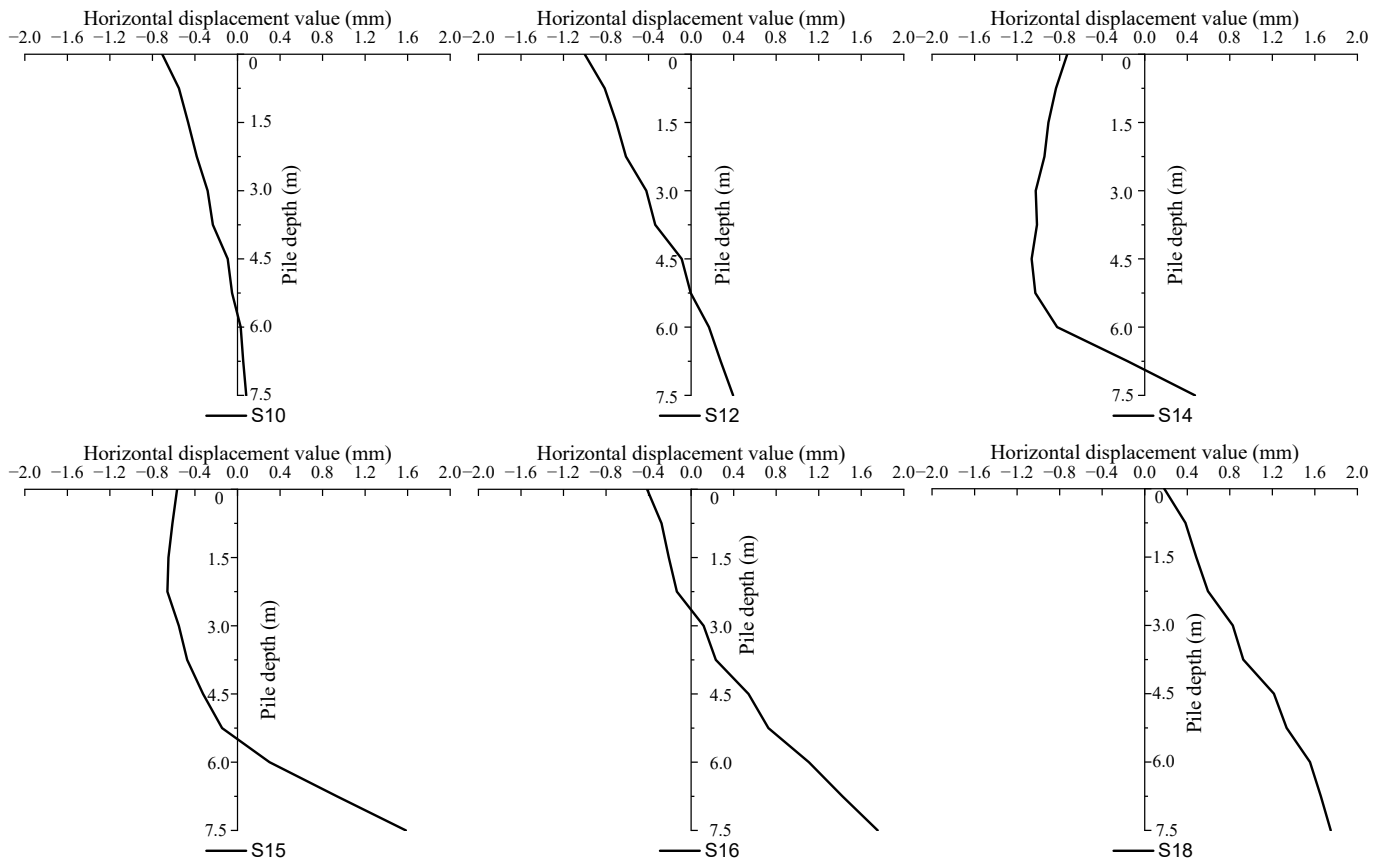
Figure 13. Horizontal displacement curve of single pile.
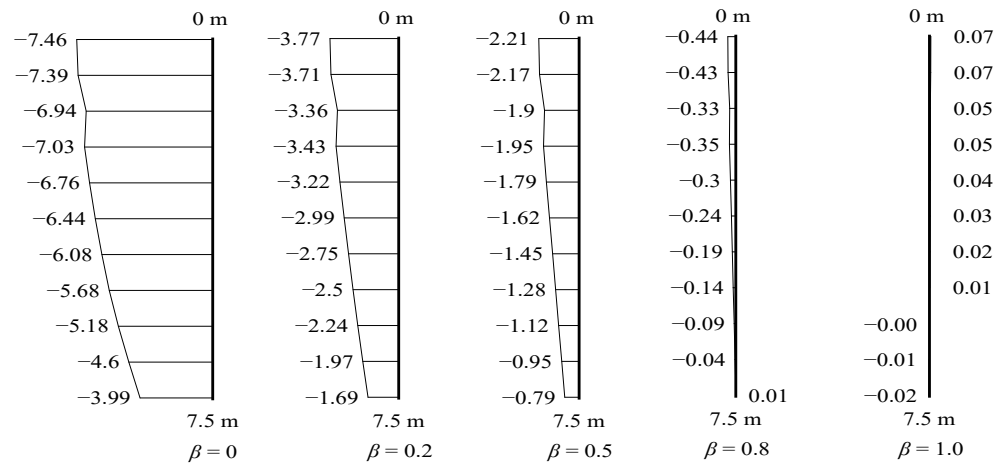

Figure 14. Final horizontal displacement diagram of single pile (mm).

(4)   Pile Shaft Force Analysis

Three construction sections (S14–S16), before and after the underpass, were selected to analyze the axial force variation of pile five during the construction of the shield underpassing the bridge piles in the palm surface at different β values, and the results are shown in Figure 15. The axial force distribution of the pile before underpassing was approximately the same: the compressed area spanned 4/5 of the length below the pile top, and the partially tensioned area spanned 1/5 of the length above the pile end. When the shield was under penetration, the pile's axial force distribution was changed further when β ≤ 0.8 at the palm surface; the entire pile body was under tension at this time. When the shield

completed the crossing, part of the area within a distance equal to 1/5 of the length below the top of the pile became axial pressure again. When the β value of the palm surface was close to one, the pile became an end-bearing pile, the axial force distribution of the pile was not changed considerably during the shield penetration, and only a small amount of axial tension appeared at the end of the pile.
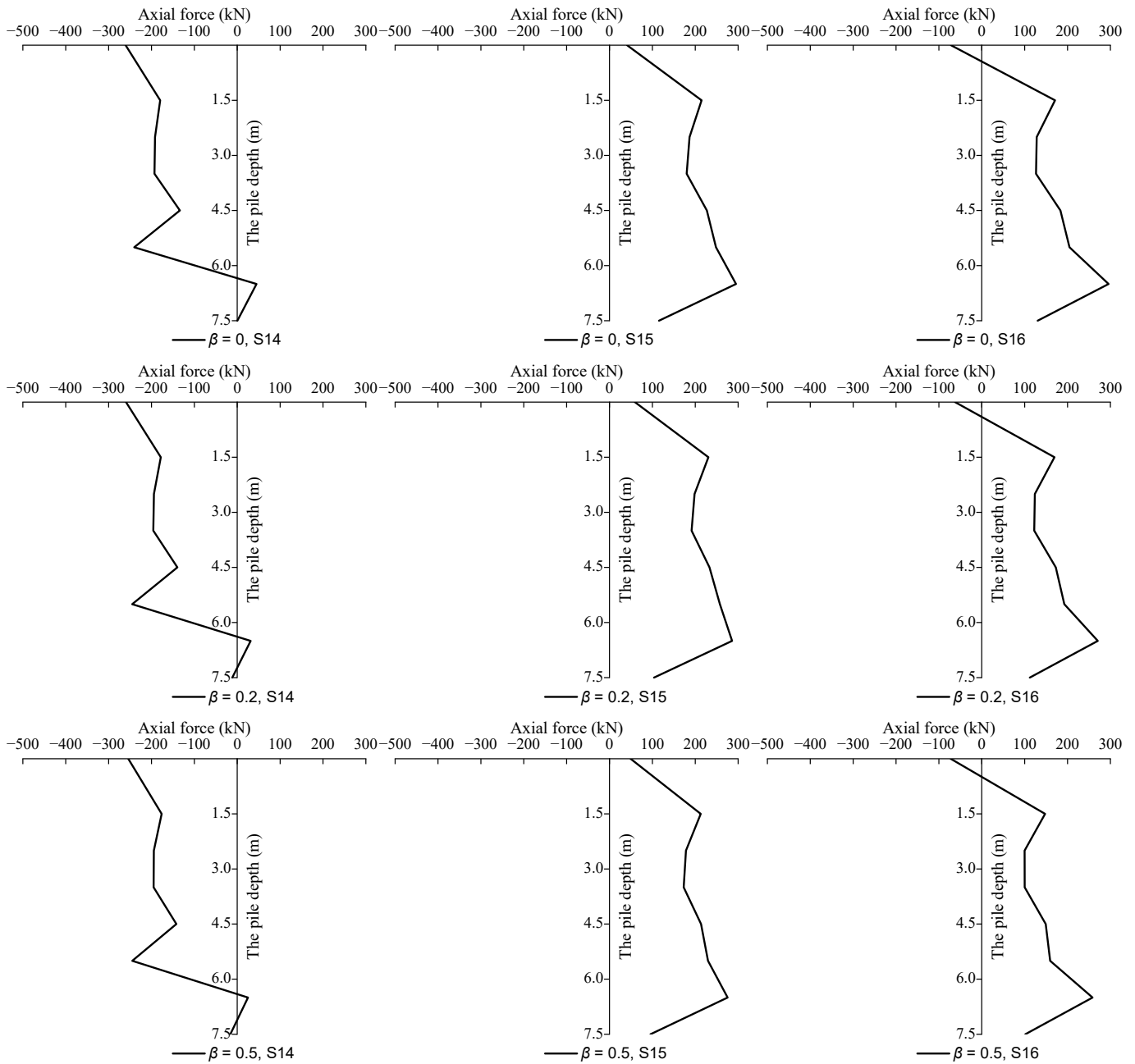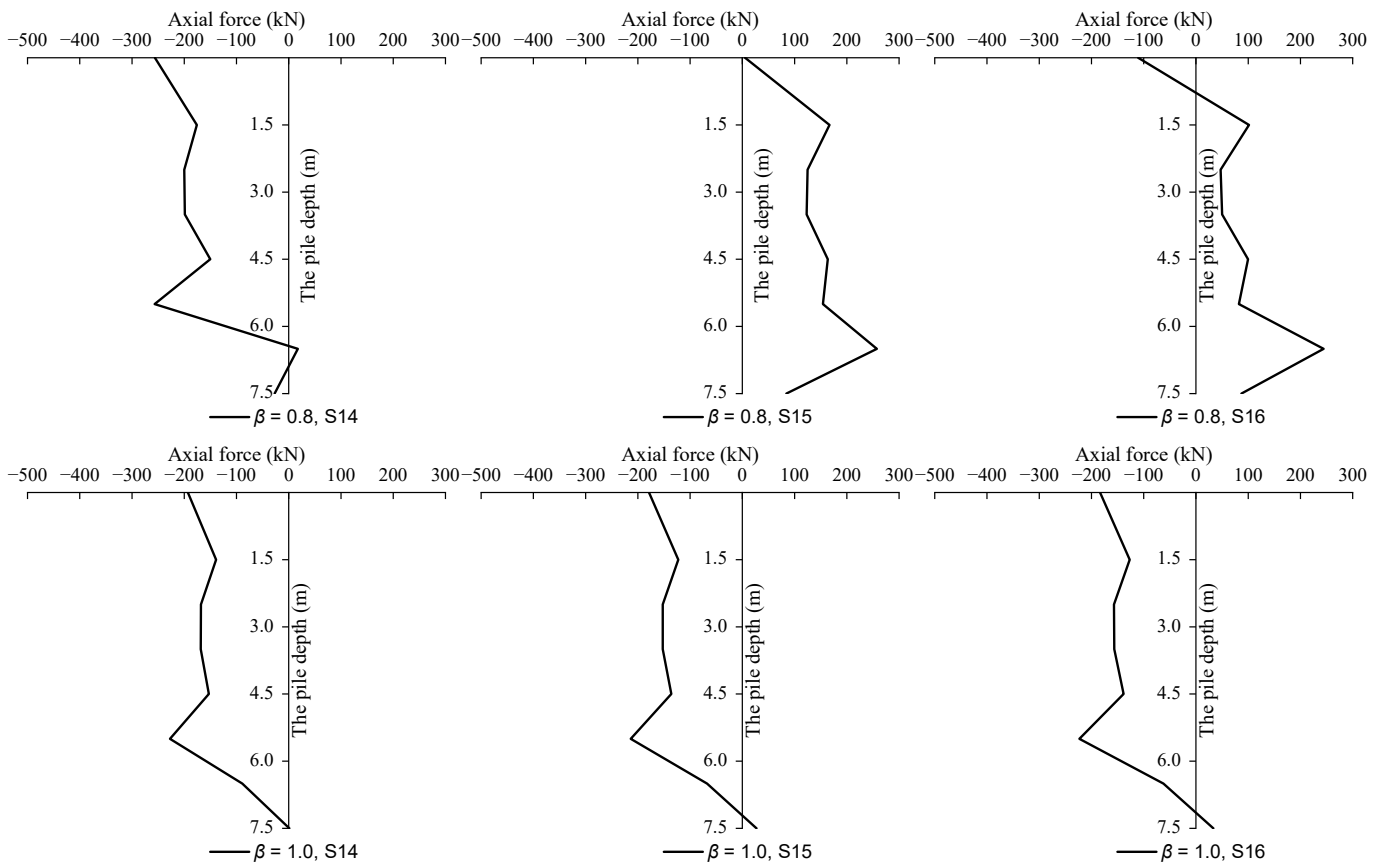

Figure 15. *Cont.*

Figure 15. Shaft axial force curve of single pile.

(5) Pile Bending Moment Analysis

Three construction sections (S14–S16), before and after the underpassing, were selected to analyze the bending moment variation of pile foundation No. 5 during the construction of the shield underpassing with different pile top loads, and the results are shown in Figure 16.
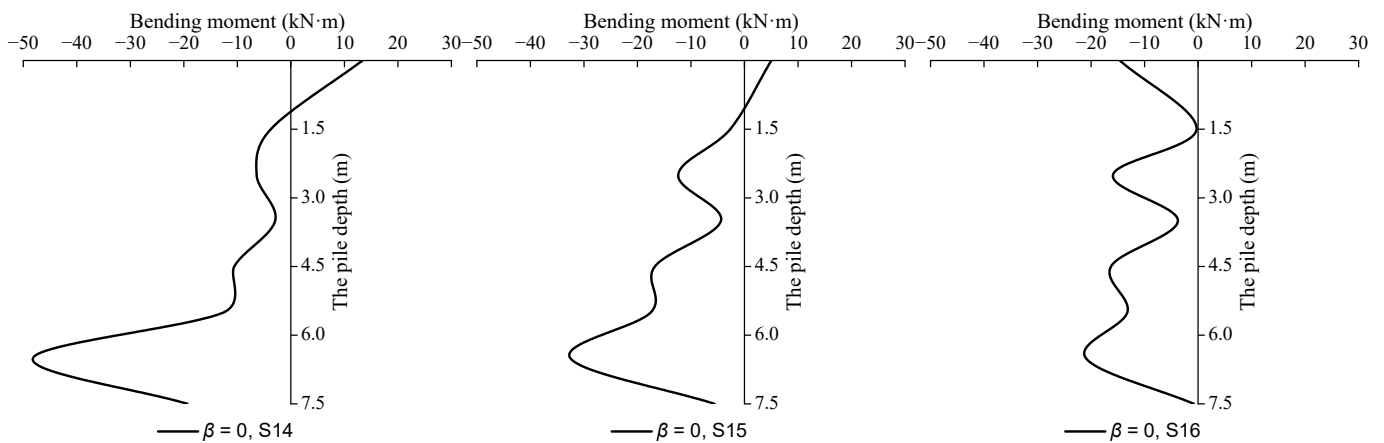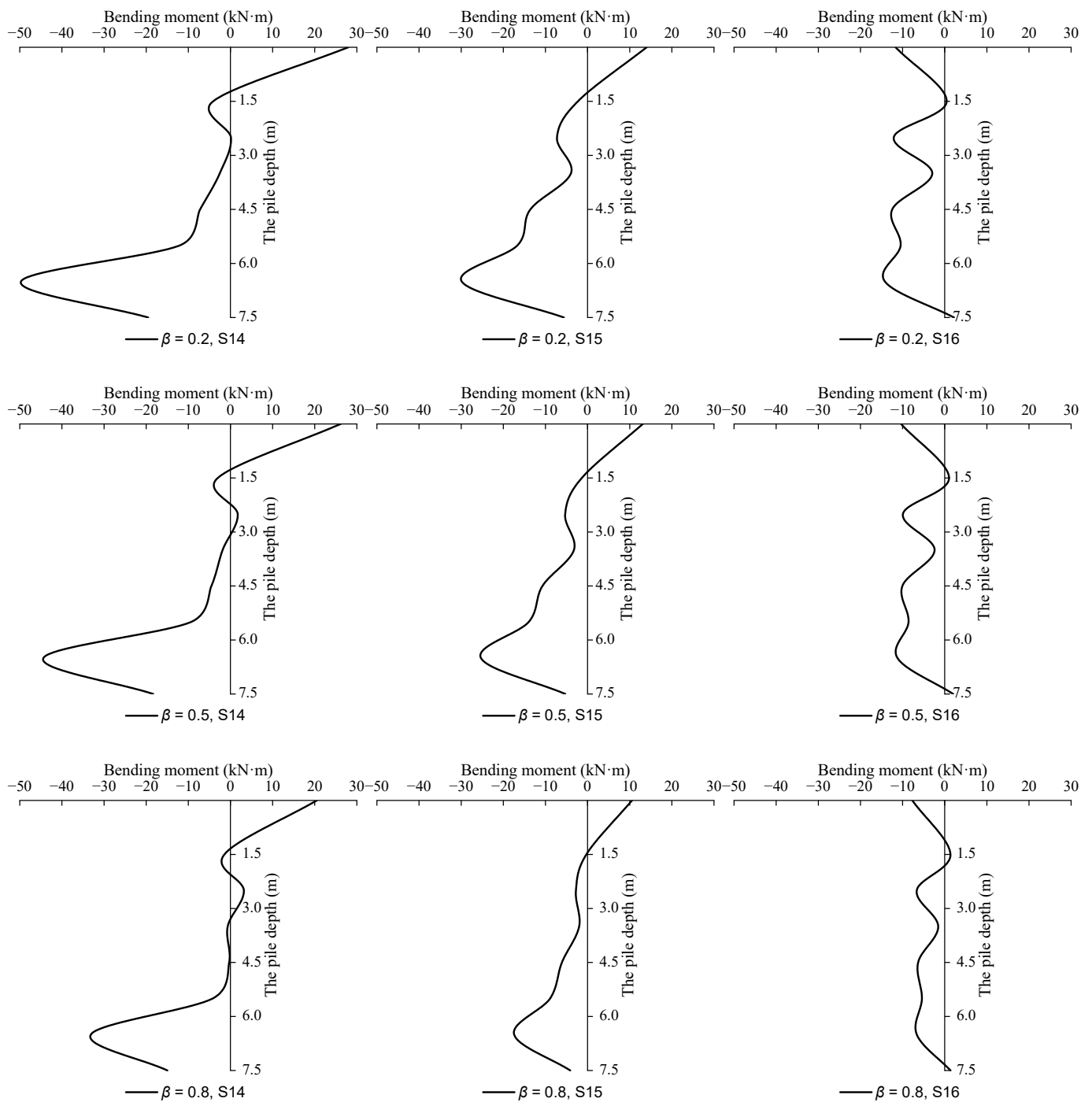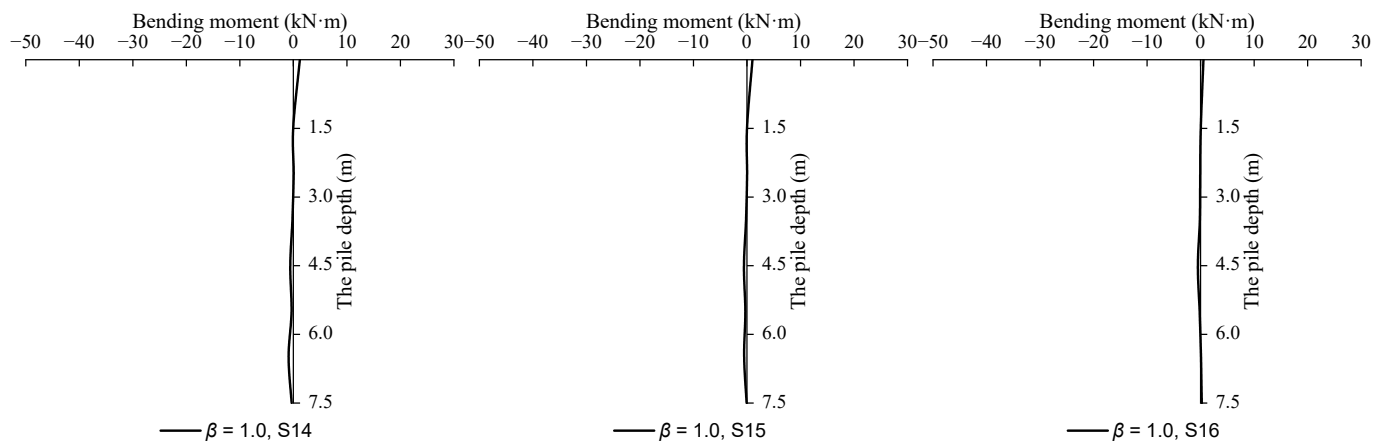

Figure 16. *Cont.*

Figure 16. *Cont.*

Figure 16. Bending moment curve of single pile.

Before the underpassing, the pile bending moment distribution is approximately the same: the pile top, at regions which are at distances lower than 1/5 of its length, exhibits tension in regions far from the left pile-base side, and within regions at distances equal to 4/5 of its length above the pile end, it exhibits tension near the left pile-base side. The comparison shows that the bending moment at both ends of pile No. 5 is significantly influenced by the β value of the palm surface. In the cases of $\beta = 0$ and $\beta = 1$, the pile top bending moment was smaller than that of the other cases. This phenomenon can be explained as follows. A pile is subjected to an additional horizontal load owing to the disturbance of the upper soil caused by excavation, reducing the bending moment at both ends of the pile. Furthermore, the final distribution of the bending moment of the pile is not significantly related to the value of β.

Several calculations were conducted to further analyze the stress level of the piles obtained by considering the combination of the shaft axial force and bending moment. The results not presented here indicate that the maximum tensile stress of 4.83 MPa was obtained when $\beta = 0$ before underpassing, which can be mitigated by applying loads on the top of the pile, as explained in Section 5.

5. Mechanical Response of Shield Underpassing Pile Foundation under Different Pile Top Loads

Pile top loads p of 100 kPa, 200 kPa, and 400 kPa are applied to the pile top bearing at the shield boring face with a hard-rock height ratio of $\beta = 0.5$, and the influential analysis of the surface settlement, monopile displacement variation, and monopile internal force variation caused by the construction of the shield underpassing bridge piles under different pile top loads, p, is carried out.

(1)   Surface Settlement Analysis

The final ground surface settlement value curves for the two measurement lines Y1 and Y2 are shown in Figures 17 and 18, respectively.
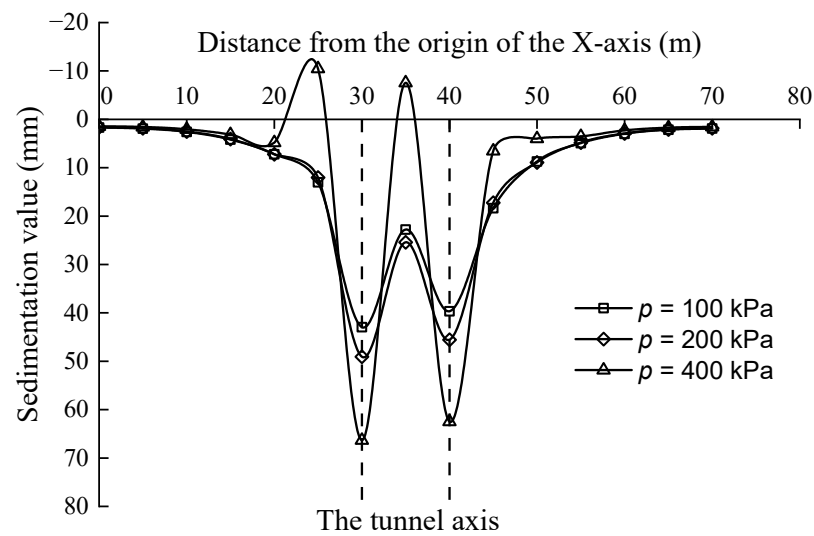
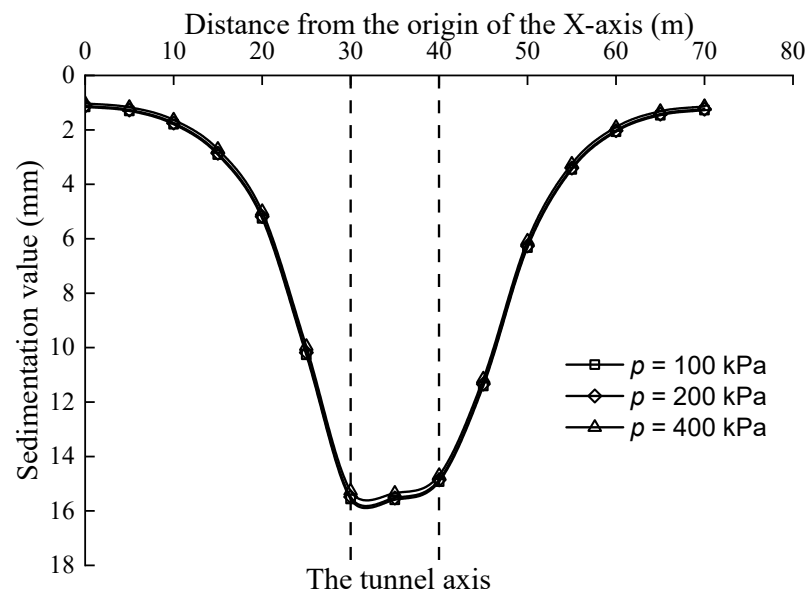**Figure 17.** Surface subsidence curve of line Y1.

Figure 18. Surface subsidence curve of line Y2.

From the curves, it can be seen that within the underpassing area, the surface above the left and right tunnels have obvious settlement troughs. Specifically, the greater the pile top load, the greater the surface settlement value, the deeper the depth of the surface settlement trough, and the wider the surface area caused by settlement. Outside the underpassing area, a settlement trough appears in the middle of the surface above the left and right tunnels, and the settled surface is not affected by the increase in the pile top load. In addition, within the underpassing area, when p increases to 400 kPa, the depth of the ground settlement trough is substantially deeper than before, and the ground surface uplifts in the local area, which indicates that the shield underpassing the bridge pile with an excessive pile top load might trigger the cracking of the ground in the underpass area.

Furthermore, in the case of p = 400 kPa, the maximum surface uplift in the local area near the left pile cap reached 10.48 mm, whereas the maximum surface subsidence directly below the left tunnel axis was up to 66.55 mm (Figure 17), both exceeding the allowable values listed in Table 2. Generally, for the three load levels mentioned above, the maximum vertical displacements of the strata within the underpassing area exceeded the previously set allowable values. Therefore, construction disturbances should be taken seriously when underpassing piles in composite strata with similar proportions of hard and soft rocks.

(2)   Single-Pile Settlement Analysis

Pile 5 of the right bearing in Figure 6 is selected for the analysis of the monopile settlement, and the variation in the pile top settlement as the shield penetration construction proceeded is shown in Figure 19. From the figure, it can be seen that when the shield is dug beyond 6 m behind the pile foundation, no settlement occurs in the pile foundation. When the shield is dug within the range of 3–6 m behind the pile foundation, a small amount of settlement occurs in the pile foundation. When the shield is dug within 3 m behind the pile foundation, the settlement of the pile foundation accelerates with the approach of the shield panel and remains after the shield crossing, and the settlement value of the pile foundation stabilizes after the shield passes through the pile foundation for 9 m. In addition to this, the higher the pile top load, the greater the settlement of the pile foundation caused by the construction of the underpass pile foundation.

Furthermore, it can be observed that the settlement values of all cases in Figure 19 are smaller than that of Figure 12, which indicates that loads applied on piles contribute to disturbance control.
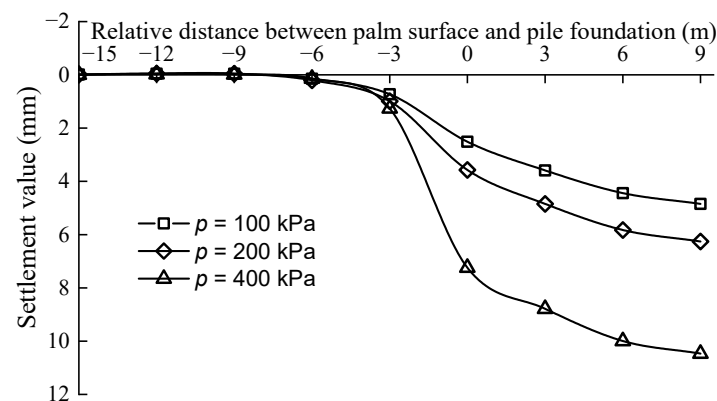

Figure 19. Single pile tip settlement curve.

(3)   Analysis of Horizontal Displacement of Single Pile

The final horizontal displacement caused by the shield underpassing the bridge piles with different pile top loads are shown in Figure 20. After the shield was fully excavated, pile five moved towards the direction of the left line tunnel (X-axis negative direction) at all locations, and the displacement decreased with an increase in the pile depth. In addition, a comparison between Figures 14 and 20 indicates that the construction disturbance improved, whereas this enhancement decreases with an increase in the pile top load. However, in the cases presented here, stratum reinforcement is still required for safety.
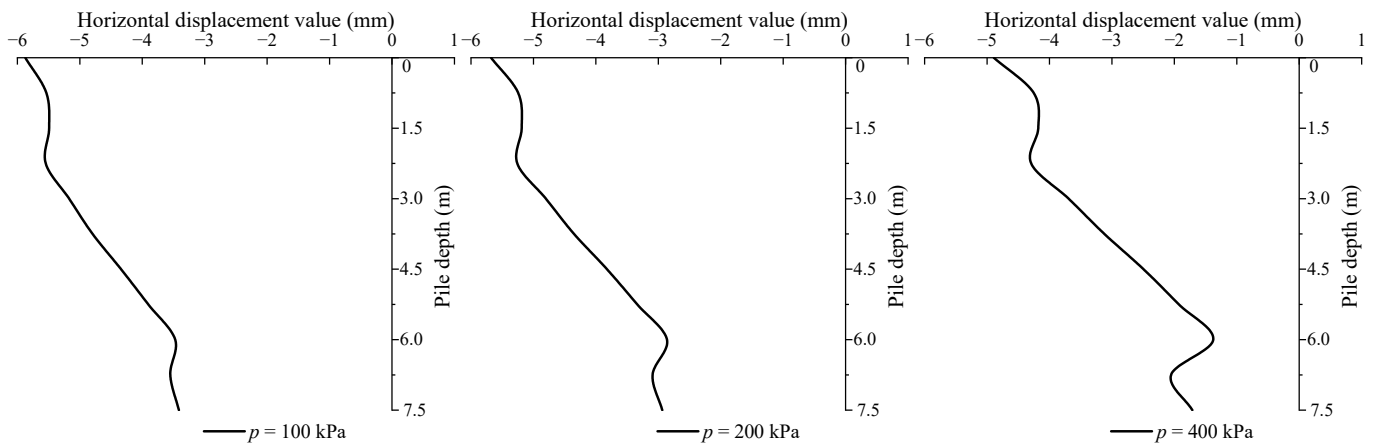
Figure 20. Horizontal displacement curve of single pile.

(4) Pile Shaft Force Analysis

Three construction sections (S14~S16), before and after underpassing, were selected to analyze the axial force variation of pile foundation No. 5 during the construction of the shield underpassing with different pile top loads, and the results are shown in Figure 21. The pile shaft force was significantly affected by the pile top load, and the larger the pile top load, the larger the pile shaft force. The construction of the shield underpassing causes the axial force of pile foundation No. 5 to become smaller, but the pile does not show the area of axial tension.
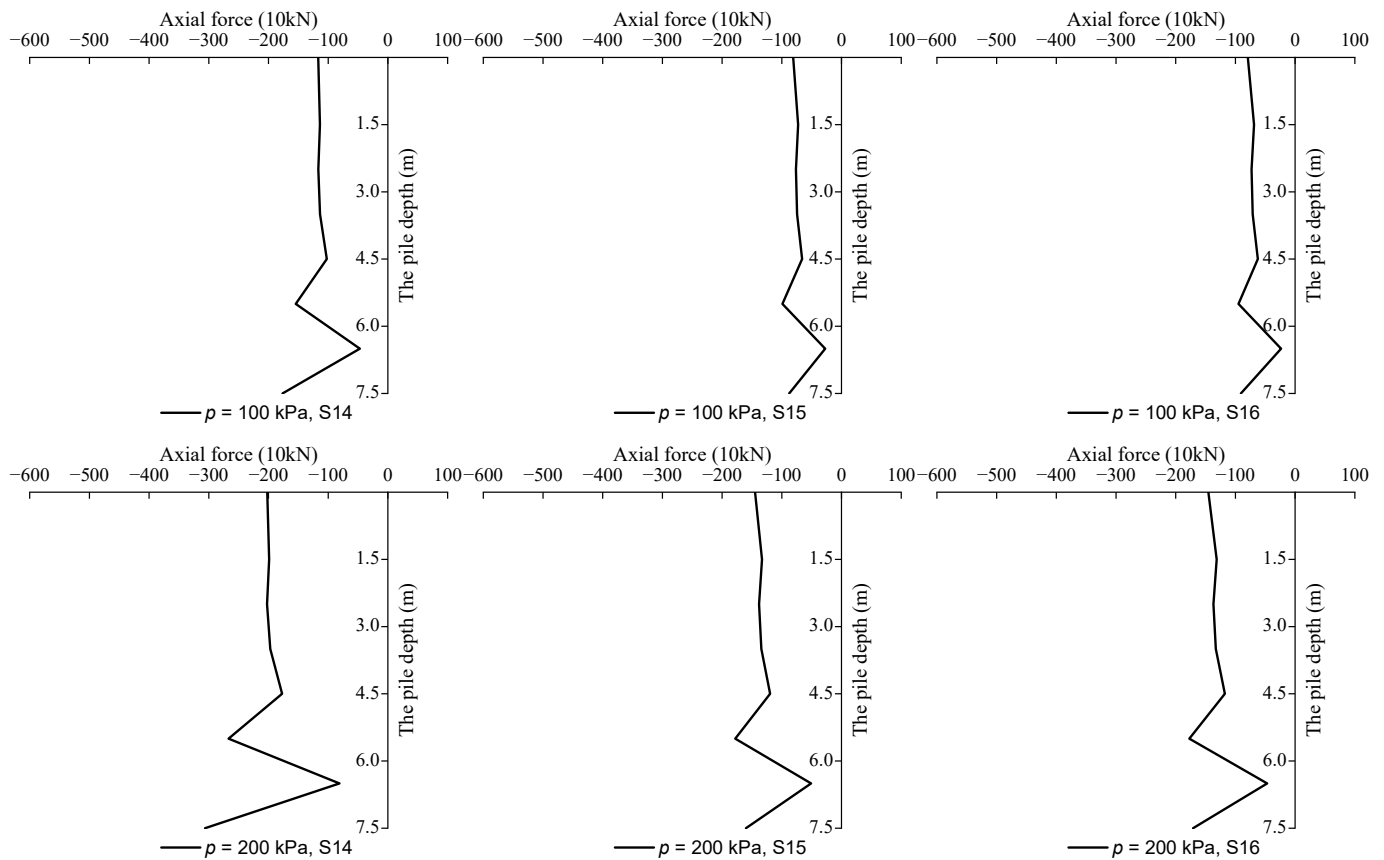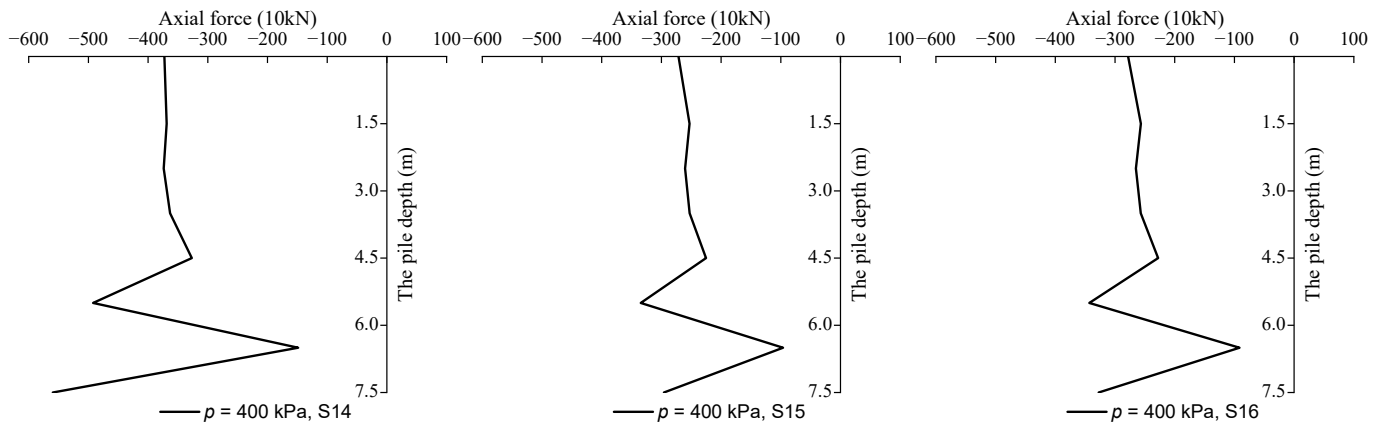

Figure 21. *Cont.*

Figure 21. Shaft axial force curve of single pile.

(5) Pile Bending Moment Analysis

Three construction sections, S14–S16, before and after underpassing, were selected to analyze the bending moment variation of pile foundation No. 5 during the construction of the shield underpassing with different pile top loads, and the results are shown in Figure 22. Before the underpassing, the pile bending moment distribution was approximately the same: the pile top at regions which were at distances lower than 1/5 of its length exhibited tension in regions far from the left pile-base side, and within regions at distances equal to 4/5 of its length above the pile end, it exhibited tension near the left pile-base side. The bending moment of the pile top was affected considerably by the pile top load, and the value of the pile top bending moment increased as the pile top load increased. When underpassing through, the pile ends all exhibited tension away from the left pile-base side, and the pile's end-moment value of the pile base (at a higher pile top load) was larger. When the shield passed through the pile foundation, the bending moment at the pile end increased further, and the rate of increase of the bending moment increased as a function of the load on the pile top.
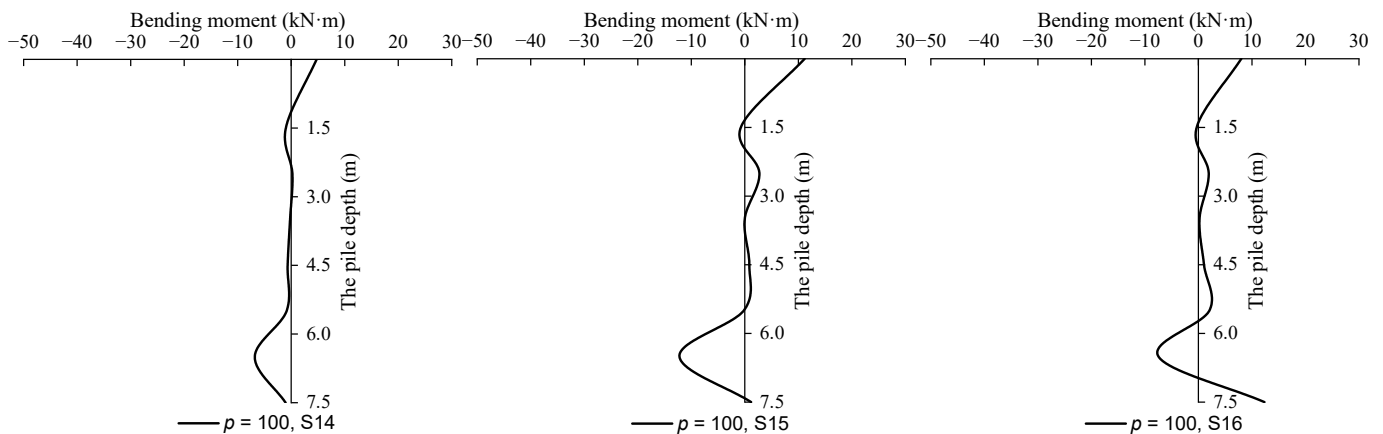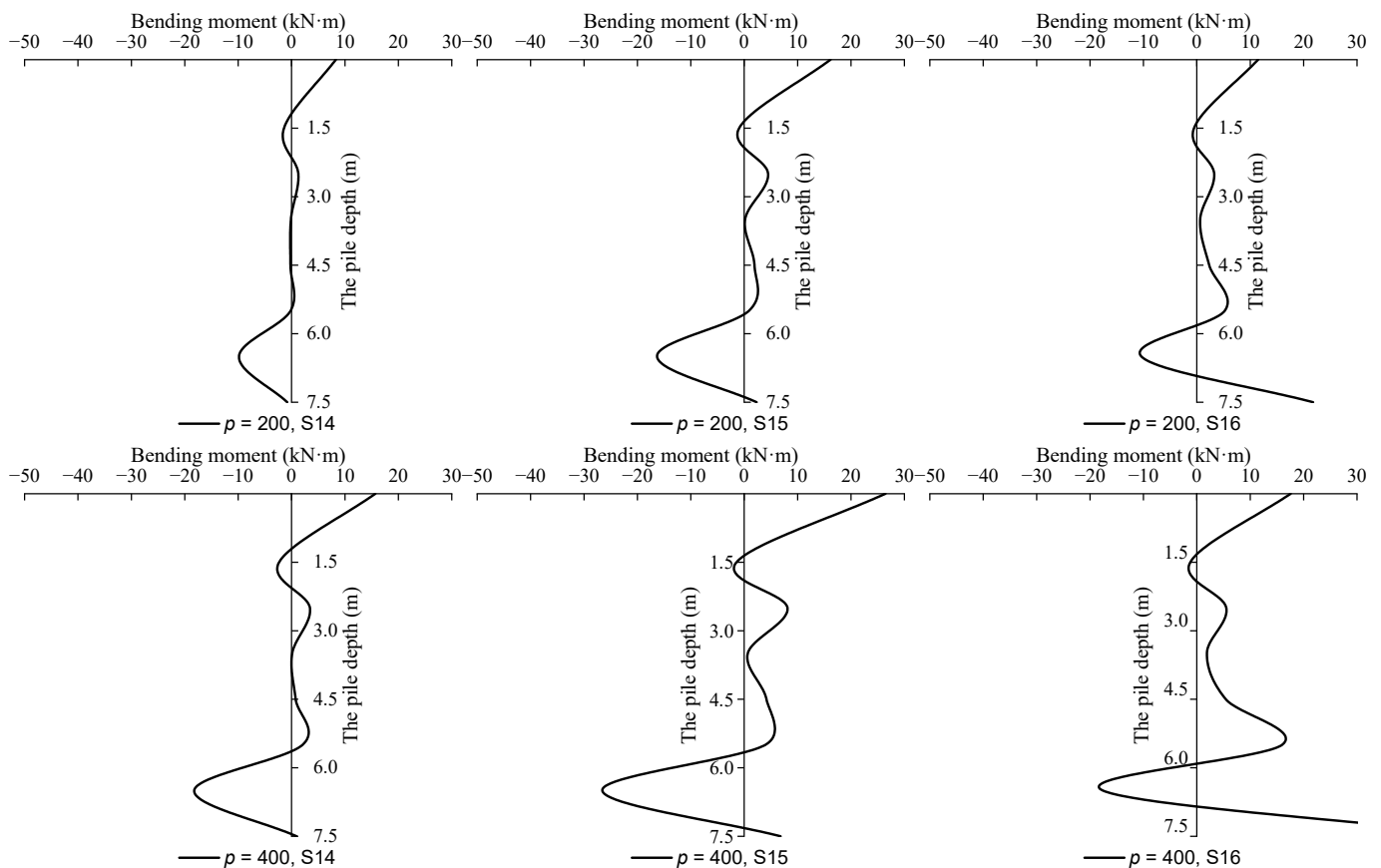

Figure 22. *Cont*.

Figure 22. Bending moment curve of single pile.

The stress state was obtained through a cross-section analysis to further analyze the mechanical response of a single pile under different load levels. After calculations, the maximum tensile stress was 1.87 MPa, which was obtained in the case of $p = 400$ kPa during underpassing. Compared with the allowable magnitude of the stress level, the stresses of each section of the pile were lower than the allowable value, which was set to be 1.98 MPa, according to the requirements for structural performance.

6. Conclusions

The mechanical responses of the shield underpassing the bridge piles at different pile top loads in strata with different hard-rock height ratios were investigated in this study. A finite element model was established to analyze the variation patterns of the surface settlement, single-pile displacement, and the internal force generated during shield construction under different conditions. The main conclusions are as follows.

1. The ground surface above the existing bridge piles exhibited significant sensitivity. When additional stresses were ignored, the width and depth of the surface subsidence increased as the hard-rock ratios decreased, and the maximum settlement was within the determined allowable range. In addition, when the pile top load was significant, the local uplift and excessive surface settlement increased the risk of ground cracking and collapse.

2. The influence area of the single-pile settlement was mainly within 9 m from the single pile to the palm surface. In addition, the load applied to the piles reduced the settlement, but increased the horizontal displacement of a single pile. However, the increasing effect on the horizontal displacement decreased with an increase in the load.

3. The internal force of a single pile is significantly influenced by the pile top load. The analysis showed that as the pile top bending moment increased, the pile axial tension

induced by shield construction decreased. This indicates that the appropriate amount of top load improved the pile deformation caused by shield construction.

4. Construction disturbance was maintained within the allowable range for hard-rock height ratios greater than or equal to 0.8. Therefore, monitoring measures and foundation reinforcements should be adjusted promptly according to the variation in the actual stratigraphic distribution in the upper-soft and lower-hard composite strata.

7. Further Development

In engineering practice, the actual stratum distribution is highly uneven, and the interfaces of different strata are typically curved. In addition, the relative positions of the tunnel axis and piles are more complex than those adopted in the proposed simulations. Therefore, effort must be made to establish a more general model to obtain more accurate results.

References

1. Ng, C.; Fong, K.; Liu, H. The effects of existing horseshoe-shaped tunnel sizes on circular crossing tunnel interactions: Three-dimensional numerical analyses. *Tunn. Undergr. Space Technol.* **2018**, *77*, 68–79. [CrossRef]
2. He, Z.; Li, C.; He, Q.; Liu, Y.; Chen, J. Numerical Parametric Study of Countermeasures to Alleviate the Tunnel Excavation Effects on an Existing Tunnel in a Shallow-Buried Environment near a Slope. *Appl. Sci.* **2020**, *10*, 608. [CrossRef]
3. Li, S.; Li, P.; Zhang, M.; Liu, Y. Influence of Approaching Excavation on Adjacent Segments for Twin Tunnels. *Appl. Sci.* **2019**, *10*, 98. [CrossRef]
4. Li, X.L.; Wang, B.L.; Li, X.; Ji, C. Analysis of Anti-Floating Measures and Construction Parameters of Shield Tunnel through River under Ultra-Shallow Covering. *Appl. Mech. Mater.* **2013**, *2545*, 628–634. [CrossRef]
5. Xu, H.Q.; Xiao, C.J.; Liu, W.L.; Zuo, Y.Z.; Wei, C.Q. Numerical Study on Karst Treatment Technology of Wuhan Metro Line 6. *IOP Conf. Ser. Earth Environ. Sci.* **2020**, *571*, 012090. [CrossRef]
6. Qiu, J.; Liu, H.; Lai, J.; Lai, H.; Chen, J.; Wang, K. Investigating the Long-Term Settlement of a Tunnel Built over Improved Loessial Foundation Soil Using Jet Grouting Technique. *J. Perform. Constr. Facil.* **2018**, *32*, 04018066. [CrossRef]
7. He, S.; Lai, J.; Li, Y.; Wang, K.; Wang, L.; Zhang, W. Pile group response induced by adjacent shield tunnelling in clay: Scale model test and numerical simulation—ScienceDirect. *Tunn. Undergr. Space Technol.* **2022**, *120*, 104039. [CrossRef]
8. Li, Z.; Chen, Z.; Wang, L.; Zeng, Z.; Gu, D. Numerical simulation and analysis of the pile underpinning technology used in shield tunnel crossings on bridge pile foundations. *Undergr. Space* **2020**, *6*, 396–408. [CrossRef]
9. Al-Omari, R.R.; Al-Soud, M.S.; Al-Zuhairi, O.I. Effect of Tunnel Progress on the Settlement of Existing Piled Foundation. *Studia Geotech. Mech.* **2019**, *41*, 102–113. [CrossRef]
10. Wu, H.N.; Zhang, P.; Chen, R.P.; Lin, X.T.; Liu, Y. Ground Response to Horizontal Spoil Discharge Jet Grouting with Impacts on the Existing Tunnels. *J. Geotech. Geoenviron. Eng.* **2020**, *146*, 05020006. [CrossRef]
11. Zhao, C.; Lei, M.; Shi, C.; Cao, H.; Yang, W.; Deng, E. Function mechanism and analytical method of a double layer pre-support system for tunnel underneath passing a large-scale underground pipe gallery in water-rich sandy strata: A case study. *Tunn. Undergr. Space Technol. Inc. Trenchless Technol. Res.* **2021**, *115*, 104041. [CrossRef]
12. Li, Y.; Zhang, W. Investigation on passive pile responses subject to adjacent tunnelling in anisotropic clay. *Comput. Geotech.* **2020**, *127*, 103782. [CrossRef]
13. Ma, W.; Liu, J.; Zhang, L. Analysis of the impact of large-diameter shield construction adjacent to the side of the pile foundation. *IOP Conf. Ser. Earth Environ. Sci.* **2021**, *634*, 012109. [CrossRef]
14. Mirsepahi, M.; Nayeri, A.; Lajevardi, S.H.; Mirhosseini, S.M. Effect of multi-faced twin tunneling in different depths on a single pile. *Innov. Infrastruct. Solut.* **2021**, *6*, 42. [CrossRef]
15. Mo, P.Q.; Marshall, A.M.; Fang, Y. Cavity Expansion-Contraction-Based Method for Tunnel-Soil-Pile Interaction in a Unified Clay and Sand Model: Drained Analysis. *Int. J. Geomech.* **2021**, *21*. [CrossRef]
16. Loganathan, N.; Poulos, H.G.; Stewart, D.P. Centrifuge model testing of tunnelling-induced ground and pile deformations. *Géotechnique* **2000**, *50*, 283–294. [CrossRef]

17. Huang, K.; Sun, Y.W.; Zhou, D.Q.; Li, Y.J.; Jiang, M.; Huang, X.Q. Influence of water-rich tunnel by shield tunneling on existing bridge pile foundation in layered soils. *J. Cent. South Univ.* **2021**, *28*, 2574–2588. [CrossRef]

18. Soomro, M.A.; Mangi, N.; Xiong, H.; Kumar, M.; Mangnejo, D.A. Centrifuge and numerical modelling of stress transfer mechanisms and settlement of pile group due to twin stacked tunnelling with different construction sequences. *Comput. Geotech.* **2020**, *121*, 103449. [CrossRef]

19. Boonsiri, I.; Takemura, J. Observation of Ground Movement with Existing Pile Groups Due to Tunneling in Sand Using Centrifuge Modelling. *Geotech. Geol. Eng.* **2015**, *33*, 621–640. [CrossRef]

20. Abuallan, F.M.; Jusoh, S.N.; Sohaie, H.; Marto, A.; Mohamad, H.; Rahim, A. Physical model on effects of tunnelling towards single piles under zoned of influence. *IOP Conf. Ser. Mater. Sci. Eng.* **2021**, *1144*, 012100. [CrossRef]

21. Soomro, M.A.; Ng, C.W.W.; Liu, K.; Memon, N.A. Pile responses to side-by-side twin tunnelling in stiff clay: Effects of different tunnel depths relative to pile. *Comput. Geotech.* **2017**, *84*, 101–116. [CrossRef]

22. Ng CW, W.; Lu, H. Effects of the construction sequence of twin tunnels at different depths on an existing pile. *Can. Geotech. J.* **2014**, *51*, 173–183.

23. Wood, D.M. *Soil Mechanics*; Cambridge University Press: Cambridge, UK, 2009.